Vol 13 No 12, December 2004
1009-1963/2004/13(12)/2141-06

Chinese Physics

© 2004 Chin. Phys. Soc.
and IOP Publishing Ltd

Theoretical study of quantum confined Stark shift in InAs/GaAs quantum dots*

Guo Ru-Hai(郭汝海), Shi Hong-Yan(时红艳), and Sun Xiu-Dong(孙秀冬)†

Department of Applied Physics, Harbin Institute of Technology, Harbin 150001, *China*

(Received 1 June 2004; revised manuscript received 4 August 2004)

The quantum confined Stark effect (QCSE) of the self-assembled InAs/GaAs quantum dots has been investigated theoretically. The ground-state transition energies for quantum dots in the shape of a cube, pyramid or "truncated pyramid" are calculated and analysed. We use a method based on the Green function technique for calculating the strain in quantum dots and an efficient plane-wave envelope-function technique to determine the ground-state electronic structure of them with different shapes. The symmetry of quantum dots is broken by the effect of strain. So the properties of carriers show different behaviours from the traditional quantum device. Based on these results, we also calculate permanent built-in dipole moments and compare them with recent experimental data. Our results demonstrate that the measured Stark effect in self-assembled InAs/GaAs quantum dot structures can be explained by including linear grading.

Keywords: quantum dots, plane-wave expansion, self-assembled, quantum confined Stark effect
PACC: 7320D, 7115T, 3260S

1. Introduction

Progress made in the growth of "free-standing" (e.g., colloidal) quantum dots and in the growth of semiconductor-embedded ("self-assembled") dots has opened the door to new and exciting spectroscopic studies of quantum structures. The last decade has witnessed an intensive research effort focused on the physics of semiconductor quantum dots. Self-assembled InAs–GaAs quantum dots provide nearly ideal examples of zero-dimensional semiconductor systems[1−4] and are hence of considerable contemporary interest for the study of new phenomena and potential device applications. However, very little has been known about their detailed atomic and electronic structures, including, for instance, the form of the ground-state electron and hole wavefunctions. Therefore, to model and hence to control the optical and electronic properties, precise knowledge on a level as fundamental as the electronic structure would be desirable. Initial structural studies of uncapped Stranski–Krastinow (SK) dots suggested a pyramidal shape,[5] and several groups therefore conducted theoretical investigations into the structure of ideal pyramidal dots.[6−11] The typical schematic diagram of an InAs pyramidal quantum dot and InAs wetting layer is shown in Fig.1.

More recent structural study has demonstrated that both the dot shape and size can vary with the growth conditions. In addition to the ideal pyramidal shape, more recent work has also provided evidence of "truncated" pyramids,[12] lens-shaped dots,[13] cone-shaped dots,[14] and has shown that In and Ga concentrations can also vary in the dot.[15−17] These have revealed rich and sometimes unexpected features such as quantum-dot shape-dependent transitions, size-dependent (red) shifts between absorption and emission, emission from high excited levels, surface-mediated transitions, exchange splitting, strain-induced splitting, and Coulomb-blockade transitions. These new results have promoted the need for developing suitable theoretical tools capable of analysing the electronic structure of quantum dots.

The first theoretical study of the electronic properties of these structures used the single-band

*Project supported by the National Natural Science Foundation of China (Grant No 90201003), the Programme from the Ministry of Education for Distinguished Young Teacher and the Foundation of Heilongjiang Province for the Returned Overseas Chinese Scholars (Grant No LC01C11).

†E-mail: xdsun@hit.edu.cn

effective-mass theory to calculate the energy levels and wavefunctions in InAs/GaAs cone-shaped quantum dots.[14] The strain was taken to be a constant in the InAs material and zero in the surrounding GaAs barrier. More recently, the single-band theory was used for InAs/GaAs dots with a more realistic pyramidal geometry. [5] The variation of the strain in and around the InAs island was determined using the elastic continuum theory, in which the atomic nature of the constituent materials was neglected. Both approaches neglected valence-band mixing, and the strain dependence of the effective masses. Figures in most theoretical papers on ideal pyramidal dots show the presence of a permanent dipole in the dot, due to the large built-in stain fields which localize the highest-energy hole state near the bottom of the pyramid, so that it sits underneath the lowest-energy electron state in the dot. Because of the built-in dipole, quantum dot structures should exhibit an asymmetric Stark shift in the presence of an applied field. As an electric field F is applied, the transition energy $E_{\rm TR}$ between the ground-state electron and hole levels will vary quadratically as $E_{\rm TR}(F) = E_{\rm TR}(0) - pF + \beta F^2$, where $E_{\rm TR}(0)$ is the zero-field transition energy, p depends on the built-in dipole, and β is a measure of the polarizability of the electron and hole wavefunctions. Asymmetry in experimental measurements of the Stark shift has indeed revealed a built-in dipole both in InAs/GaAs,[18] and in $Al_yIn_{1-y}As/Al_xGa_{1-x}As$ quantum dots; but, surprisingly, the direction of the dipole is opposite to that predicted from the theoretical calculations, with the hole centre of mass above the electron centre of mass in both cases. Some recent theoretical works have explained this "inverted" alignment by assuming composition grading in the pyramidal InAs quantum dots.[16,17]

In this paper we carry out a theoretical investigation of the influence of different shape and size on the sign and magnitude of the built-in dipoles in quantum dots with cubical, pyramidal and "truncated" pyramidal shapes. Here we consider three kinds of common shapes of quantum dots with fixed composition, and show whether they can lead to the correct sign of the built-in dipole moment compared to that observed experimentally. The calculations are undertaken with separate one-band Hamiltonian equation for the electrons and holes. We also present a simple method for calculating strain fields in quantum dots, but neglect the anisotropy. As a result of our work, we show conclusively that the measured Stark effect in self-assembled quantum dot structures can be explained by including linear grading.

2. Method

Calculations were performed using a three-dimensional (3D) superlattice of dots, with superlattice unit cell of a size $2B_x \times 2B_y \times 2B_z$. The Schrödinger equation for the system was solved using a plane-wave envelope-function technique. The normalized envelope wavefunctions $\Psi_n(\boldsymbol{r})$ are determined by a Fourier series expansion

$$\Psi_n(\boldsymbol{r}) = \sum_k \frac{A_K^n}{\sqrt{8B_xB_yB_z}} \exp(\mathrm{i}\boldsymbol{k}\cdot\boldsymbol{r}), \qquad (1)$$

where $\boldsymbol{k} = \pi(m/B_x, n/B_y, p/B_z)$ and $\boldsymbol{r} = (x, y, z)$. We set the separation between neighbouring dots equal to the dot dimension in order to minimize cross talk, while ensuring efficient convergence of the Fourier series. We first describe here the general method and then discuss the particular form of the strained one-band Hamiltonian equations used. The Schrödinger equation here is

$$\hat{H}\,\Psi_n = E_n\,\Psi_n. \qquad (2)$$

Using the plane-wave basis, we substitute Eq.(1) in Eq.(2) and then left multiply $\exp(-\mathrm{i}\boldsymbol{k}'\cdot\boldsymbol{r})$ and integrate for a unit cell, the energy levels and eigenfunctions can be found by solving the large Hamiltonian matrix equation:

$$\sum_K \bar{H}_{k,k'} A_k^n = E_n A_{k'}^n, \qquad (3)$$

$$\bar{H}_{k,k'} = \int_r \frac{\mathrm{d}\boldsymbol{r}}{8B_xB_yB_z} \exp(-\mathrm{i}\boldsymbol{k}'\cdot\boldsymbol{r})\hat{H}(\boldsymbol{r})[\exp(\mathrm{i}\boldsymbol{k}\cdot\boldsymbol{r})]. \qquad (4)$$

In order to set up the Hamiltonian matrix of Eq.(3), we must first evaluate the matrix elements $\bar{H}_{k,k'}$ linking the plane-wave basis states of wave vectors $\boldsymbol{k}$ and $\boldsymbol{k}'$. The misfit of lattice constant between the quantum dot and matrix will generate a non-uniform strain distribution throughout the dot and the matrix. Both the electron and hole Hamiltonian equations contain terms related to this local strain distribution. The calculation of the spatial strain distribution in a quantum dot structure requires the solution of a 3D problem in elasticity theory. This is often achieved by using the finite-difference or atomistic technologies,[8,19] which require considerable computational effort. A method

based on the Green function technique for calculating strains in quantum dot structures was recently presented.[20] An analytical formula in the form of Fourier series has been obtained for the strain tensor for arrays of quantum dots of arbitrary shape by taking into account the anisotropy of elastic properties. Of equal or even greater importance, the technique is also particularly well-suited as the input to electronic structure calculations based on the envelope function method and using a plane-wave expansion technique, because the strain-dependent matrix element linking any pair of plane waves can be determined analytically. We use the above method to directly determine the strain-dependent terms in the Hamiltonian matrix. We assume, for simplicity, that the elastic constants of the dot and matrix are equal and isotropic, the values of which given in Table 1.

We derive Hamiltonian equations of the electron and hole envelope function from the one-band $\boldsymbol{k}\cdot\boldsymbol{P}$ theory.[21,22] The electron Hamiltonian is given as

$$\hat{H}_{\rm c}(\boldsymbol{r}) = -\frac{\hbar^2}{2m_0 m^*(\boldsymbol{r})}\nabla^2 + V_{\rm c} + a_{\rm c}\varepsilon_{{\rm h}y}(\boldsymbol{r}) + d_{{\rm p}z}(\boldsymbol{r}) + eFz, \quad (5)$$

where $m^*(\boldsymbol{r})$ is the electron effective mass, $V_{\rm c}$ the unstrained conduction-band edge, $a_{\rm c}\varepsilon_{{\rm h}y}(\boldsymbol{r})$ the hydrostatic deformation of the conduction band edge, and $d_{{\rm p}z}(\boldsymbol{r})$ the piezoelectric potential. The strain-induced band deformation causes the effective-mass parameters to deviate from their bulk values. The variation of the electron effective mass with the (hydrostatically) strained band gap, $E_{\rm gs}$, is given, from the three-band $\boldsymbol{k}\cdot\boldsymbol{P}$ theory, as

$$\frac{1}{m^*(\boldsymbol{r})} = 1 + \frac{2E_{\rm p}(\boldsymbol{r})}{3E_{\rm gs}(\boldsymbol{r})} + \frac{E_{\rm p}(\boldsymbol{r})}{3[E_{\rm gs}(\boldsymbol{r}) + \Delta_0(\boldsymbol{r})]} + \delta(\boldsymbol{r}), \quad (6)$$

where $E_{\rm p}(\boldsymbol{r})$ is the Kane interband energy parameter, and $\delta(\boldsymbol{r})$ takes into account the contribution of remote bands to the conduction-band effective mass.

Substituting Eq.(5) into Eq.(4), we find that the expression for $\bar{H}_{k,k'}$ has the form

$$\bar{H}_{k,k'} = \frac{1}{8B_xB_yB_z}\int_r {\rm d}\boldsymbol{r}\exp[{\rm i}\boldsymbol{k}''\cdot\boldsymbol{r}) \times \left[\frac{\hbar^2}{2m_0m^*}(k_x^2+k_y^2+k_z^2) + V_{\rm c} + a_{\rm c}\varepsilon_{{\rm h}y}(\boldsymbol{r}) + d_{{\rm p}z}(\boldsymbol{r}) + eFz\right], \quad (7)$$

where $\boldsymbol{k}'' = \boldsymbol{k} - \boldsymbol{k}'$. We define the characteristic function of the dot $\chi(\boldsymbol{r})$ in the supercell (1 for InAs, 0 for GaAs), and take the lattice mismatch of the dot ε_0 to be 6.7% for InAs in GaAs. It can be shown for an isotropic elastic medium that the Fourier transform of the real-space strain tensor component $\varepsilon_{ij}(\boldsymbol{r})$ is given by ($\boldsymbol{k}'' \neq 0$)[20]

$$\tilde{\varepsilon}_{ij}^{\rm iso}(\boldsymbol{k}'') = \varepsilon_0\tilde{\chi}(\boldsymbol{k}'')\left[\delta_{ij} - \frac{3\lambda+2\mu}{\lambda+2\mu}\frac{k_i''k_j''}{|\boldsymbol{k}''|^2}\right], \quad (8)$$

where $\lambda = C_{12}$ and $\mu = C_{44}$ are the Lamé constants for an isotropic elastic medium. $\chi(\boldsymbol{k}'')$ is the Fourier transform of the dot characteristic function.

For the case of isotropic elastic constants, to find the analytic form of $\bar{H}_{k,k'}$ is a trivial matter for all but the piezoelectric term in $\hat{H}_{\rm c}(\boldsymbol{r})$. In order to evaluate this term, we use the analytic expression of Ref.[23] for the Fourier transform of the piezoelectric potential ($\boldsymbol{k}'' \neq 0$),

$$\tilde{d}_{{\rm p}z}(\boldsymbol{k}'') = \frac{-18{\rm i}\varepsilon_0}{\alpha_0\sqrt{2\pi}}\left(\frac{C_{11}+2C_{12}}{C_{11}}\right)\left[\frac{e_{14}^{\rm bar}}{\alpha_{\rm r}^{\rm bar}}\chi(\boldsymbol{k}'')\frac{k_x''k_y''k_z''}{|\boldsymbol{k}''|^4} + \left(\frac{e_{14}^{\rm dot}}{\alpha_{\rm r}^{\rm dot}} - \frac{e_{14}^{\rm bar}}{\alpha_{\rm r}^{\rm bar}}\right)\sum_{k'''}\chi(\boldsymbol{k}'''-\boldsymbol{k}'')\chi(\boldsymbol{k}'')\frac{k_x''k_y''k_z''}{|\boldsymbol{k}''|^4}\right], \quad (9)$$

where α_0, $\alpha_{\rm r}^{\rm dot}$ and $\alpha_{\rm r}^{\rm bar}$ are respectively the permittivity of free space and the relative permittivities of the dot and barrier material, $e_{14}^{\rm dot}$ and $e_{14}^{\rm bar}$ are the piezoelectric constants.

From the experiment, Stranski–Krastanow quantum dots have a large base-to-height ratio. The kinetic energy in the x–y plane is thus reduced relative to that in the growth direction, leading to a stronger heavy-hole confinement and a weaker light-hole confinement. The one-band valence Hamiltonian we use for the hole ground state is then given as

$$\hat{H}_{\rm v}(\boldsymbol{r}) = -\frac{\hbar^2}{2m_0}\{[\gamma_1(\boldsymbol{r})+\gamma_2(\boldsymbol{r})]\nabla_{||}^2 + [\gamma_1(\boldsymbol{r})-2\gamma_2(\boldsymbol{r})]\nabla_z^2\} + V_{\rm v} + a_{\rm v}\varepsilon_{{\rm h}y}(\boldsymbol{r}) - b_{{\rm a}x}\varepsilon_{{\rm a}x}(\boldsymbol{r}) + d_{{\rm p}z}(\boldsymbol{r}) + eFz, \quad (10)$$

where $V_{\rm v}$ is the unstrained valence band-edge energy, $a_{\rm v}\varepsilon_{{\rm h}y}(\boldsymbol{r})$ the hydrostatic deformation of the valence-band edge, and $-b_{{\rm a}x}\varepsilon_{{\rm a}x}(\boldsymbol{r})$ the axial-strain-induced

shift in the heavy-hole band edge. In a similar way, we can obtain the Hamiltonian matrix of $\bar{H}_{k,k'}$ for the valence band. The calculations presented in the following are carried out by assuming the room-temperature energy gaps and effective masses. In order to correctly describe the one-band Luttinger parameters $\gamma_i(\boldsymbol{r})$, we first relate them to their eight-band counterparts, $\gamma_i'(\boldsymbol{r})$. In the full eight-band Hamiltonian, the interactions between the conduction-band minimum and valence-band maximum are considered explicitly, with $\gamma_i'(\boldsymbol{r})$ being then due to interactions with remote bands, and assumed to be independent of the built-in strain and the lowest-energy gap. The eight-band $\gamma_i'(\boldsymbol{r})$ values are related to the one-band values by[24,25]

$$\gamma_1'(\boldsymbol{r}) = \gamma_1(\boldsymbol{r}) - \frac{E_{\rm p}(\boldsymbol{r})}{3E_{\rm g}(\boldsymbol{r})},$$
$$\gamma_2'(\boldsymbol{r}) = \gamma_2(\boldsymbol{r}) - \frac{E_{\rm p}(\boldsymbol{r})}{6E_{\rm g}(\boldsymbol{r})}, \qquad (11)$$

where $E_{\rm g}$ is the unstrained band gap. The energy gap changes in a strained material, so that the one-band Luttinger parameters γ_i will also change in a strained inclusion, as

$$\gamma_1(\boldsymbol{r}) = \gamma_1'(\boldsymbol{r}) + \frac{E_{\rm p}(\boldsymbol{r})}{3E_{\rm g}(\boldsymbol{r})},$$
$$\gamma_2(\boldsymbol{r}) = \gamma_2'(\boldsymbol{r}) + \frac{E_{\rm p}(\boldsymbol{r})}{6E_{\rm g}(\boldsymbol{r})}. \qquad (12)$$

The parameters used are tabulated in Table 1. We have calculated the parameter values for InAs in a GaAs matrix, and for unstrained GaAs. So from Eq.(12), we obtain the strain-renormalized one-band effective mass of $\gamma_1 = 10.601$, $\gamma_2 = 3.253$, and m^*=0.042 which were used for the present work. Finally, we assume the values of the elastic constants for GaAs in the dot and the surrounding matrix. This assumption has been justified previously, based on Keye's scaling rule for elastic constants.[20]

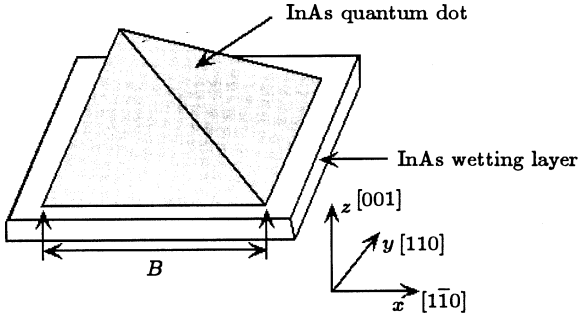


Fig.1. Schematic diagram of an InAs pyramidal quantum dot and InAs wetting layer together with axes referred to in the paper.

Table 1. Parameters used in this paper.

Parameter	InAs	GaAs
$\gamma_1^{\rm L}$	19.67	6.85
$\gamma_2^{\rm L}$	8.37	2.1
$E_{\rm g}$/eV	0.418	1.519
Δ_0/eV	0.38	0.33
$E_{\rm p}$/eV	22.2	25.7
$m^*_{\rm exp}$(0K)	0.023	0.067
$a_{\rm c}$	−5.08	−7.17
$a_{\rm v}$	1.00	1.16
$e_{14}/\varepsilon_{\rm r}/(10^{-3}{\rm cm}^{-2})$	−2.97	−12.49
$V_{\rm c}$(300K)/eV	0.621	1.428
$V_{\rm v}$(300K)/eV	0.265	0.000
$V_{\rm c} + a_{\rm c}\varepsilon_{{\rm h}y}$(300K)/eV	0.994	1.428
$V_{\rm v} + a_{\rm v}\varepsilon_{{\rm h}y}$/eV	0.192	0.000
$C_{11}/10^{10}$Pa	11.9	
$C_{12}/10^{10}$Pa	5.38	
$C_{44}/10^{10}$Pa	5.95	
b_{ax}/eV	−1.8	
$\varepsilon_{\rm r}$ (InAs)	15.15	

3. Results and discussion

Figures 2(a) and 2(b) give the variation of the ground-state electron and hole confinement energies, calculated for different shapes of quantum dots as a function of dots size with a base to height ratio equal to 2:1. The results of pyramidal quantum dots are in good agreement with previous calculation results.[6,9] We also calculate ground-state confinement energies for pyramidal, "truncated" pyramidal and cuboidal quantum dots, and find that the electron and hole confinement energies get more closely to each other when the quantum dots become more flat. Figure 3 shows the calculated difference between the electron and hole ground-state energies for the dot structure considered in Fig.1 when the electric field is applied along the z-axis. We have defined the applied field to be positive when it results in the conduction- and valence-band edges moving to the higher energy side above the dot and to the lower energy side below the dot, as illustrated in the inset of Fig.3.

It can be seen that the transition energy varies quadratically with the applied field, so that $E_{\rm TR}(F) = E_{\rm TR}(0) - pF + \beta F^2$. The linear coefficient p depends directly on the initial separation of the electron and hole mean positions, i.e. on the built-in ground-state dipole moment of the dot. The peak transition energy is seen at positive field in Fig.3, which is consistent with a negative dipole moment. Using quadratic fit in Fig.3, we obtain the dipole $d = -p/e$,

with $d = -0.82$nm. By contrast, experimental Stark shift measurements both on InAs/GaAs (Ref.[18]) and $In_xGa_{1-x}As/Al_xGa_{1-x}$ As quantum dot structures show the peak transition energy at negative fields. The experimentally observed built-in dipole is therefore of opposite sign to that predicted from Fig.3, with the hole–electron separation $d = 0.40 \pm 0.1$nm in Ref.[18]. There must be some reasons to account for this great difference. Changing from a cuboidal to a pyramidal geometry, the increasing anisotropy of the dot shape modifies the axial strain fields. Consequently, the heavy holes are moved from the top surface of the dot toward the dot base, so that the ground-state hole moves more rapidly than the ground-state electron, and the space of hole–electron separation increases. Observation from the TEM experiment indicates the shape of a dot tapering from the base to the top. The heavy-hole potential at the top can be deeper than that at the base if the dot includes indium gradient, i.e. forms an In_xGa_{1-x} As alloy, with the indium concentration, x, increasing from the base to the top.

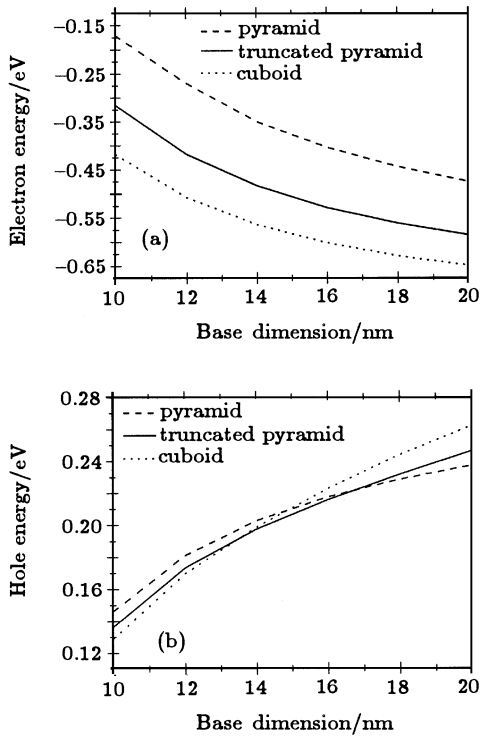


Fig.2. Ground-state electron and hole confinement energies (300K) as functions of dot size for InAs quantum dots of base/height =2:1; pyramidal quantum dots (dashed line), "truncated" pyramidal quantum dots—truncated factor f=0.75 (solid line), and cuboidal quantum dots (dotted line).

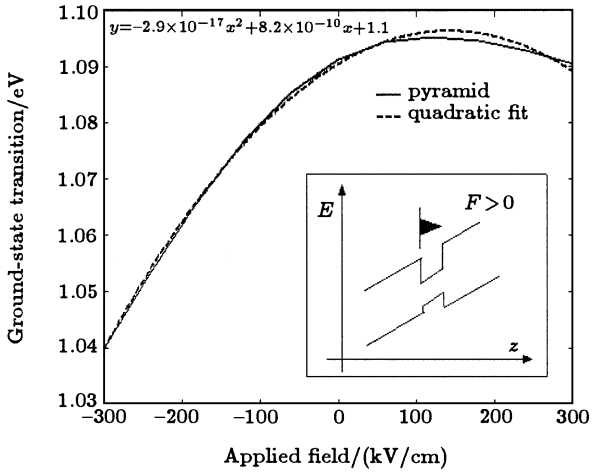


Fig.3. Ground-state transition energy (300K) as a function of applied field for pyramidal dot with base 12nm and height 6nm. The solid line shows the theoretical results and the dashed line shows the quadratic fit to it. Inset: variation of the band edge with position for $F > 0$.

We therefore conclude that the structure of these buried Stranski–Krastinow grown dots must be greatly different from an ideal constant composition pyramid, and now turn to consider what kind of dot structures can be consistent with the experimentally observed sign of dipole. Figure 4 shows the calculated dipole in a "truncated" pyramidal dots of base width B=18 nm and height H=5.5 nm as a function of "truncated" factor, f. The value assumed for H is the same as the value estimated from a TEM analysis of uncapped dots.[18] Here f represents the fraction of the total pyramid height removed so that the height of the full pyramid is 22nm. According to the experimental results, if the hole is seated at the upper part of the dot, and above the electron, we require a deeper heavy-hole potential at the top of the dot than at the base. Increasing "truncated" factor f makes the space of electron–hole smaller and inclusion of indium gradient will deepen the heavy-hole potential further. So we have assumed a linear composition gradient for simplification of calculation, but recent work suggests that the true composition profile may be more complicated.[17] The solid line shows a linear graded cube, for which d=0 when x=1 at the base, with the d increasing to a maximum value ~0.7nm near $x \sim 0.3$ at the base. A similar trend is observed for the "truncated" pyramid with f=0.75 (dashed line). For smaller composition gradient, the increasing indium component will push the hole downwards slightly faster than the electron and with increasing indium component the electron will move more rapidly than the hole, finally reach the

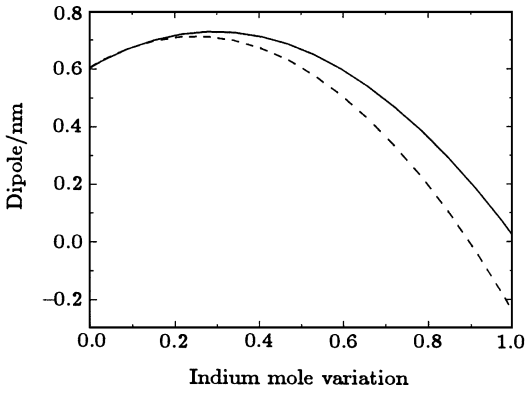


Fig.4. Dipole (300K) as a function of composition gradient for dots of base 18nm and height 5.5nm, graded from $In_xGa_{1-x}As$ at the base to InAs at the top of the surface. The solid line are results for cuboidal dots (f=1), and the dashed lines are results for "truncated" pyramidal dots (f=0.75).

position below the hole. It is very clear that if we only consider the level of truncation, the mean position of the electron will always remain above the hole, even changing to a cubical dot (f=1). We can see from Fig.4 that the correct sign of dipole can be obtained by including the composition gradient. The electron initially is located above the hole, but the positions reverse with increasing gradient. We have omitted the influence of the wetting layer because the grading must be stronger in the presence of the wetting layer. As we know, Li *et al* also studied the optical transitions and quantum-confined Stark effects of self-assembled InAs/GaAs quantum dots in the framework of effective-mass envelope-function theory.[26,27] Their results based on quantum dots of cylindrical shape showed that the transition energy will decrease as the size of InAs/GaAs dots increases, and the energy spectrum shows clear redshifts in electric field; these results have the similar trend to our results.

4. Conclusion

In this article, we have used an efficient plane-wave envelope-function technique to determine the ground-state electronic structure of quantum dots with three kinds of shapes. We have presented a method based on a Green function approach to calculate strain distributions in and around quantum dots. We have indicated that this calculation method is also particularly suited as an input step in calculations of the electronic structures of quantum dots, and also used one-band electron and hole Hamiltonian equations to investigate the different factors influencing the magnitude and sign of the built-in dipole in strained quantum dots, and also demonstrated that the built-in strain will always lead the centre of mass of the hole to lie below the centre of mass of the electron in a fixed composition dot with common shapes– cuboid, pyramid and truncated pyramid. The calculated dipole moment is of opposite sign to that determined from recent quantum-confined Stark effect experimental measurements. Our calculated results demonstrate conclusively that the measured Stark effect in self-assembled InAs/GaAs quantum dots with different shapes can only be explained theoretically by including composition gradient.

References

[1] Weller H and Eychmiiler A 1996 *Semiconductor Nanoclusters* edited by P. V. Kamat and D. Meisel, **103** 5 (Elsevier, New York)
[2] Overbeek J T G 1982 *Adv. Colloid I. Sci.* **15** 251
[3] Feng D H, Jia T Q and Xu Z Z 2003 *Chin. Phys.* **12** 1016
[4] Tabuchi M, Noda S and Sasaki A 1992 *Science and Technology of Microscopic Surfaces* edited by S. Namba, C. Hamaguchi and T. Ando, 379 (Spinger, Tokyo)
[5] Grundmann M, Stier O and Bimberg D 1995 *Phys. Rev.* B **52** 11969
[6] Stier O, Grundmann M and Bimberg D 1999 *Phys. Rev.* B **59** 5688
[7] Williamson A J and Zunger A 1999 *Phys. Rev.* B **59** 15 819
[8] Cusack M A, Briddon P R and Jaros M 1996 *Phys. Rev.* B **54** R2300
[9] Cusack M A, Briddon P R and Jaros M 1998 *Physica* B **253** 10
[10] Chang K and Xia J B 1997 *Solid State Commun.* **104** 351
[11] Ruvimov S *et al* 1995 *Phys. Rev.* B **51** 14766
[12] Ledentsov N N *et al* 1995 *Phys. Rev.* B **54** 8743
[13] Moison J M *et al* 1994 *Appl. Phys. Lett.* **64** 196
[14] Marzin J Y *et al* 1994 *Solid State Commun.* **92** 437
[15] Kegel I *et al* 1999 *Europhys. Lett.* **45** 222
[16] Liu N, Tersoff J, Baklenov O, Holmes A L and Shih C K 2000 *Phys. Rev. Lett.* **84** 334
[17] Sheng W D and Leburton J P 2001 *Phys. Rev.* B **63** 161301
[18] Fry P W *et al* 2000 *Phys. Rev. Lett.* **84** 733
[19] Benabbas T, Francois P, Androussi Y and Lefebvre A 1996 *J. Appl. Phys.* **80** 2763
[20] Andreev A D, Downes J R, Faux D A and O'Reilly E P 1999 *J Appl. Phys.* **86** 297
[21] Barker J A and O'Reilly E P 1999 *Physica* E **4** 231
[22] Bastard G 1988 *Wave Mechanics Applied to Semiconductor Heterostructures* (Halstead, New York)
[23] Davies J H 1998 *J. Appl. Phys.* **84** 1358
[24] Pidgeon C R and Brown R N 1966 *Phys. Rev.* **146** 575
[25] Meney A T, Gonul B and O'Reilly E P 1994 *Phys. Rev.* B **50** 10893
[26] Li S S *et al* 1996 *Phys. Rev.* B **54** 11575
[27] Li S S and Xia J B 2000 *J. Appl. Phys.* **88** 7171